Bulletin of the Seismological Society of America, Vol. 103, No. 5, pp. 2645–2656, October 2013, doi: 10.1785/0120120362

Reference *S*-Wave Velocity Profile and Attenuation Models for Ground-Motion Prediction Equations: Application to Japan

by Valerio Poggi, Benjamin Edwards, and Donat Fäh

Abstract Defining the reference rock or soil condition related to ground-motion prediction is an important aspect of seismic-hazard analysis. In a previous study by the authors, a method was proposed to establish a reference rock profile for Switzerland through the comparison of empirical amplification functions with shear-wave velocity profiles at 27 selected sites of the Swiss National Seismic Network. The retrieved velocity profile served as reference for a regional ground-motion prediction equation. However, a lacking piece of information remained: the anelastic attenuation for such a reference profile. Reference attenuation is essential to correctly model and interpret amplification at high frequencies. In the present study we extended our approach to simultaneously model both the reference shear-wave velocity profile and the corresponding attenuation for Japan. We compared site-specific attenuation measurements with quarter-wavelength average velocities at 36 soil and rock sites from the Japanese KiK-net strong-motion network. The selected sites are characterized by a lack of observed resonance phenomena in order to avoid trade-off between amplification and attenuation effects. We establish a parametric model through regression analysis. The resulting model gives us the possibility to estimate anelastic attenuation of a rock site with a given velocity profile and provides the base for host-to-target adjustments of real or modeled ground motion.

Introduction

The definition of a common soil or rock reference is a key issue in probabilistic seismic-hazard analysis (PSHA), in microzonation studies, local site-response analysis, and, more generally, when predicted or observed ground motion is compared for sites of different characteristics. A scaling procedure, which accounts for a common reference, is then necessary to avoid bias induced by the differences in the local geology. Without a proper correction, an under- or overestimation of the true amplification might result. Nowadays methods requiring the definition of a reference condition (e.g., PSHA) generally prescribe the characteristic of a rock reference, calibrated using indirect estimation methods based on geology or on surface proxies (e.g., Borcherdt, 1994). In most cases, a unique average shear-wave velocity value is prescribed (e.g., $V_{S30} = 800$ m/s; Dobry *et al.*, 2000; Delavaud *et al.*, 2012) as for class A of Eurocode 8 (European Committee for Standardization, 2004), assuming therefore either a homogeneous half-space or no significant increase in velocity with depth. Such a simplification, however, appears to be inappropriate if an accurate modeling of the amplification behavior over a wide frequency range is needed. For instance, in the case of subsequent microzonation or site-specific studies, such a simple reference for the underlying PSHA model (or products thereof) leads to the introduction of significant epistemic uncertainty when we attempt to deconvolve regional-site and reapply local-site amplification and attenuation effects. Some attempts at defining the whole shape of a reference rock velocity profile have been described (e.g., Boore and Joyner, 1997; Atkinson and Boore, 2006). However, often such generic profiles are used without a clear physical justification of how such a selection was performed (e.g., Drouet *et al.*, 2010). Moreover, in spite of its relevance in affecting the high-frequency part of the spectrum, the definition of the associated reference attenuation is in most cases missing or, when present, still remains quite uncertain (Van Houtte *et al.*, 2011).

In this study we propose a technique to simultaneously model the characteristics of the shear-wave velocity profile and the corresponding attenuation of a regional rock reference. The method is an extension of the approach originally proposed by Poggi *et al.* (2011) for Switzerland and is here applied to Japan. The method is based on the comparison between empirical amplification functions from spectral modeling of earthquakes (Edwards *et al.*, 2013) and average velocities computed using the quarter-wavelength (QWL) approach (Joyner *et al.*, 1981). In the original work, however, only the elastic part of the amplification spectrum was analyzed to infer the shear-wave velocity structure of the local

rock reference, while the anelastic contribution was not considered. In this study, the full amplification spectrum is used to build a parametric model based on the QWL velocity and to predict the site-dependent attenuation operator kappa (κ; Anderson and Hough, 1984) of the reference.

For the analysis we make use of a selection of 36 stiff-soil and rock sites from the Japanese KiK-net strong-motion network, for which a measured velocity profile was made available from the National Research Institute for Earth Science and Disaster Prevention (NIED; Aoi *et al.*, 2004). The selection was driven by the need to exclude sediment sites with a strong resonance behavior, where the reverberation of trapped waves in the uppermost low-velocity layers might bias the separation of the site-dependent attenuation part of the amplification spectrum. For each selected station, elastic and anelastic empirical amplification functions have been established by means of the spectral modeling technique, calibrated over the whole network. 1879 earthquake events have been used for the model calibration, with Japan Meteorological Agency magnitude (M_{JMA}) range between 2.4 and 7.3. Event use was, however, limited to a maximum M_w 6.2 in the case of elastic amplification determination to help avoid potential nonlinear site effects. For each selected site, then, a QWL representation of the shear-wave velocity profile was derived to complement the amplification and attenuation terms.

The clear advantage of using the QWL method is that it provides a frequency-dependent estimation of the average velocity at the site, as the averaging depth varies linearly with the wavelength of interest. At a given frequency, it is then possible to relate a unique amplification factor from the local amplification function to a single velocity estimate. This is certainly not obvious with standard travel-time methods to compute average velocity, such as the widely used "travel-time average velocity over the first 30 m" (V_{S30}; as prescribed by NEHRP, Building Seismic Safety Council, 2003). By comparing elastic amplification and velocity samples using the QWL approach over a number of sites, it is then possible to identify and extract those velocity values corresponding to unitary amplification, which is the nonamplifying reference baseline of the local network (Poggi *et al.*, 2011). Finally, the ensemble of all extracted QWL velocities over a range of frequencies provides a simple representation of the nonamplifying reference velocity model for the network, which can be subsequently expressed in a more suitable velocity-versus-depth representation by means of a simple inversion procedure as demonstrated by Poggi *et al.* (2011).

The analysis of the anelastic contribution to the amplification spectrum is performed in a subsequent and separate step. At first, intrinsic attenuation is disaggregated from the anelastic amplification function by using the frequency-independent (and site-dependent) attenuation operator κ (equivalent to κ_0 in Anderson and Hough, 1984). By then comparing the dependency of κ with the QWL velocity at selected KiK-net sites, a frequency-dependent predictive equation is established to model the attenuation characteristics of any arbitrary rock or stiff-soil velocity profile. Finally, the predictive equation can be used to obtain an estimate of the attenuation operator κ for the Japanese reference model obtained in the first step.

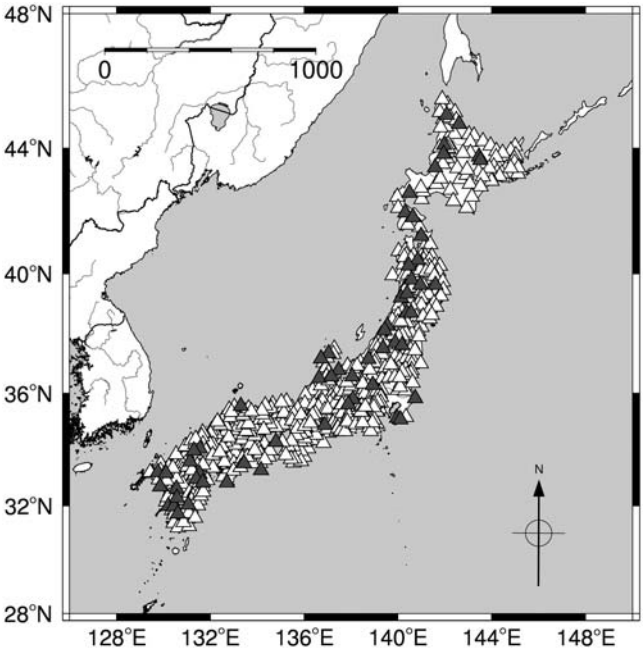

Figure 1. Station distribution of the Japanese KiK-net network. White triangles show the complete network of 689 stations. Dark gray triangles are the selected 36 soil and rock sites, characterized by the absence of observed resonances and strong amplification.

As a more general application, the result of this analysis can be used to model the site-dependent attenuation for any rock or stiff-soil site for which an estimation of the velocity profile or its corresponding QWL velocity representation is available. As an additional output of the present study, for the case where a full velocity profile does not exist, we also propose a simplified method to estimate κ from V_{S30}. We provide an example of such predictions for a range of V_{S30} velocities up to 2000 m/s. This result is then compared with the prediction obtained for Japan using a complementary approach based on a direct $V_{S30}-\kappa$ correlation, and the differences are then discussed.

KiK-Net Data Selection

Because of the large number of recordings at magnitudes of engineering interest and the abundance of available *S*-wave velocity profiles, it was decided to use data from the Japanese KiK-net strong-motion database (Aoi *et al.*, 2004) for this study. This gives us the possibility of obtaining robust statistics on the parameters that will be analyzed in this framework. The KiK-net strong-motion network (Fig. 1) consists in a total of 689 station locations: for each site a borehole is available, which accommodates three sensor installations, an accelerometer at the surface, and an accelerometer and a short-period seismometer at the bottom of the borehole. From the borehole logging, a shear-wave velocity

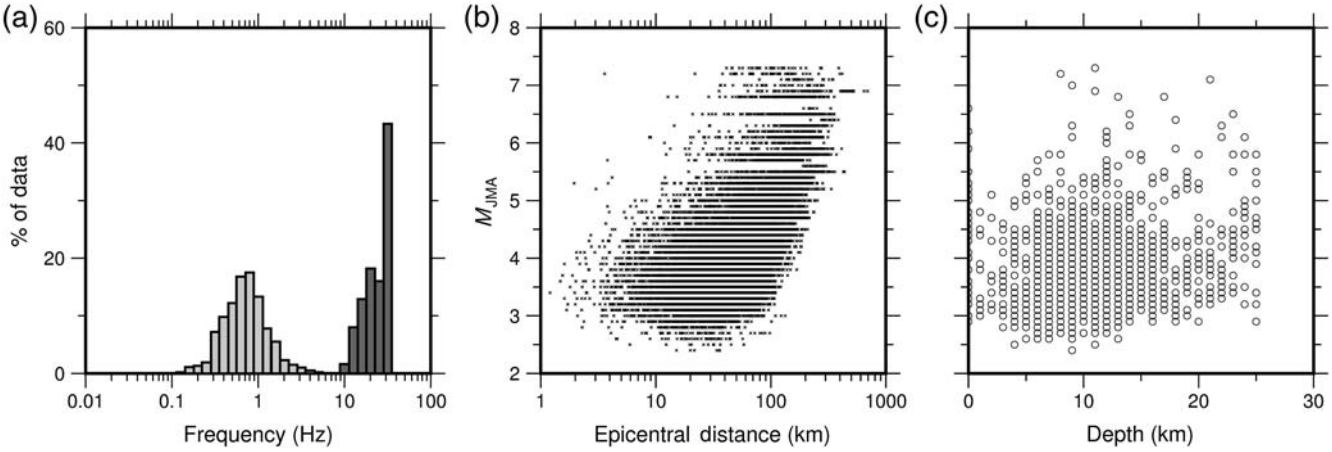

Figure 2. (a) Minimum and maximum frequencies for the spectra of the 1879 events from the Japanese network; distribution of magnitude versus (b) distance and (c) depth.

profile was made available at each location by the NIED. No uncertainty estimate is available for these profiles.

For the determination of site amplification at the KiK-net sites we follow the approach of Edwards *et al.* (2013; summarized in the Site-Specific Anelastic Amplification Functions section). They presented a method for the recovery of site-specific amplification, showing that the recovery of both elastic and anelastic amplification, including resonance phenomena, was consistent with standard spectral-ratio and 1D-*SH* modeling techniques when accounting for a network-common reference velocity profile. Because Edwards *et al.* (2013) showed that resonance effects did not bias the determination of amplification functions (e.g., through parameter trade-off), we did not need to limit sites to those without resonance behavior: in fact doing this was found to lead to unstable regressions. As a result, a total of 1879 crustal events (hypocentral depth less than 25 km) with M_{JMA} between 2.4 and 7.3 were available. The minimum and maximum frequencies used along with the distribution of M_{JMA} versus distance and depth are shown in Figure 2. For the determination of the absolute amplitude of the elastic amplification a maximum magnitude of M_w 6.2 was imposed along with a restriction that each event included in the analysis must be recorded on at least 10 stations (881 events), while each site included must have at least 10 recordings from these events (435 sites). This was in order to maximize azimuthal coverage and limit radiation and directivity effects. Of the combination of 881 events and 435 sites, a total of 18,601 spectra (geometric mean of the horizontal components) were used.

From the whole dataset with available V_S profiles and amplification and attenuation information (435 sites; Fig. 1), a selection of 36 sites was then made, representative of stiff-soil and rock site conditions, based on the reliability of the profile. The sites were selected based on the shape of the amplification function through comparison of the fundamental frequencies of resonance (f_0) directly estimated from the recordings and by indirect modeling methods using the velocity profile (see Poggi *et al.* [2012] for a comprehensive description of the selection procedure). All of the sites were manually examined, and stations showing a clear observed resonance and large amplification below 10 Hz were discarded. The removal of sites exhibiting resonance phenomena assures that the attenuation parameter κ can be given by the integral of travel time divided by the depth-dependent attenuation parameter Q over the whole path or part of the path (e.g., Anderson *et al.*, 1996), minimizing the effect of waves propagating upward and downward in resonating layers. For all the 36 selected profiles, QWL velocity curves were then produced.

The Quarter-Wavelength Average Velocity

The QWL technique is a method to compute travel-time average velocities (V_S^{QWL}) from a 1D soil velocity profile. A feature of the method is that averaging depth (z) in not prescribed *a priori*—as for the worldwide widely used V_{S30}—but is variable as a function of frequency (f), being equal to one-fourth of the wavelength (λ) of interest:

$$V_S^{QWL} = f\lambda = 4fz. \tag{1}$$

The computation of the QWL average velocity (V_S^{QWL}) is nevertheless not straightforward. In a heterogeneous velocity model and at a given frequency, the wavelength is a function of the average velocity, which is also the unknown to be determined. The problem can then be solved recursively, by minimization of the following:

$$\text{argmin}_{z(f)} \| z(f) - \frac{V_S^{QWL}(f)}{4f} \|, \tag{2}$$

given that the travel-time averaging is expressed as

$$V_S^{QWL}(f) = z(f)\left[\int_0^{z(f)} \frac{1}{V_s(z)}\, dz\right]^{-1}. \tag{3}$$

The clear advantage of this method is that the frequency-dependent estimation of the average velocity can easily be

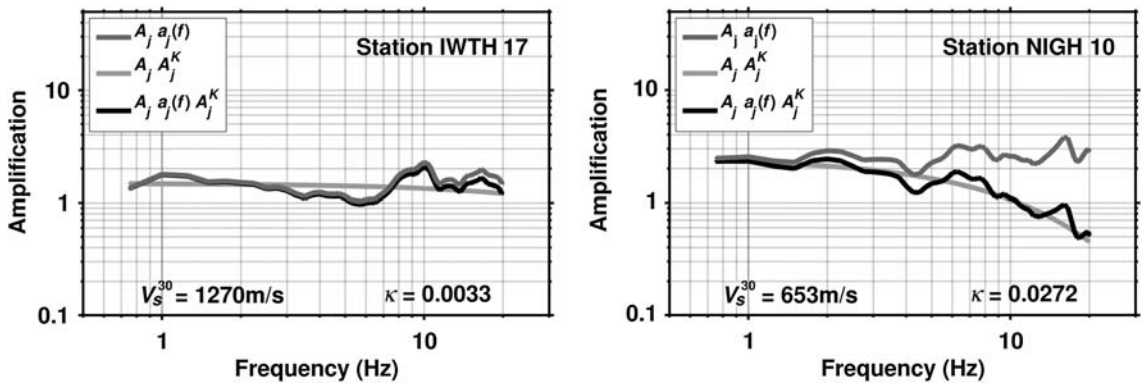

Figure 3. Examples of empirical amplification functions of (a) a typical rock site and (b) stiff-soil site of the Japanese KiK-net network. The attenuation function A^{κ} is presented in light gray, the purely elastic part in dark gray, and the viscoelastic amplification function in black for comparison.

related to other frequency-dependent parameters, such as the anelastic amplification function (e.g., Poggi *et al.*, 2011) or the vertical-over-horizontal spectral ratio of the ground motion (e.g., Edwards, Poggi, and Fäh, 2011; Poggi *et al.*, 2012). This approach is also convenient because it gives a direct representation of how the wavefield "sees" the soil structure at different wavelength scales. In practice, the high frequencies are mostly affected by the variability on the uppermost part of the soil profile, while conversely the low frequencies sample the velocity structure over greater depths. The method can therefore be considered a multiresolution approach to compute average velocities.

It should be noted that the V_{S30} is a special case of the V_S^{QWL} representation, when $z = 30$ m and, therefore, $\lambda = 4z = 120$ m. The corresponding averaging frequency is nevertheless not defined *a priori*, but instead depends on the average velocity itself, according to equation (1), as

$$f = \frac{V_{S30}}{120}. \tag{4}$$

Site-Specific Anelastic Amplification Functions

Empirical amplification functions for each site of the Japanese network were determined following Edwards *et al.* (2013). The method can be considered as the analysis of site-specific ground-motion residuals relative to spectral modeling of a large number of earthquake recordings (e.g., Edwards *et al.*, 2008; Poggi *et al.*, 2011). We assume the Fourier spectrum of the recorded ground velocity of earthquake i at station j is given by

$$\Omega_{ij}(f,r) = 2\pi f E_i(f, M_{0i}, f_{ci}) B_{ij}(f, t^*_{ij}) S_{ij}(r, r_{0\ldots n-1}, \lambda_{1\ldots n}) \times T_j(f, A_j, \kappa_j), \tag{5}$$

in which f is the frequency, r is the hypocentral distance, $E_i(f, M_{0i}, f_{ci})$ is the source model, $B_{ij}(F, t^*_{ij})$ is the intrinsic attenuation along the ray path, $S_{ij}(r, r_{0\ldots n-1}, \lambda_{1\ldots n})$ is the frequency independent amplitude decay with distance, and $T_j(f, A_j, \kappa_j)$ is the site-response function at the station with respect to a reference site. The source spectrum E_i is a Brune (1970, 1971) ω^2 spectrum: with event-specific corner frequency (f_c) and long-period spectral plateau defined by the seismic moment M_{0i}. We assume path specific intrinsic attenuation, and the geometric spreading function S_{ij} is described by a decay function with constant exponential decay in the form $R^{-\lambda}$, with $\lambda = 1.29$ (Atkinson and Mereu, 1992).

The local seismic amplification function (site term) can be simplified by decomposition through different contributions (e.g., Fig. 3) to

$$T_j(f, A_j, \kappa_j) = A_j a_j(f) e^{(-\pi f \kappa_j)} = A_j a_j(f) A^K_j, \tag{6}$$

in which A_j is the average site amplification relative to the yet unknown reference rock profile (the average amplification over all frequencies), $a_j(f)$ is the normalized frequency-dependent elastic site amplification function, and κ_j is the site-dependent attenuation operator (e.g., Anderson and Hough, 1984). Additionally, it is possible to represent the local site attenuation relative to the (yet unknown) attenuation of the reference site (κ_{REF}) by using $\Delta\kappa_j$:

$$\Delta\kappa_j = \kappa_j - \kappa_{\mathrm{REF}}. \tag{7}$$

This is useful when comparing the attenuation characteristics of different sites sharing the same common reference.

A nonlinear two-stage regression is used to separate the different contributions of equation (5), following Edwards *et al.* (2013), and to obtain $T_j(f, A_j, \kappa_j)$. In brief, the method aims to determine the combined path attenuation term at each site ($t^*_j + \kappa_j$), the event-common source corner frequency f_c, and the signal moment for each spectrum (a spectral-amplitude parameter). A grid search over f_c along with a nonlinear search for the remaining two parameters is used. A regional attenuation model is not used to predetermine $t^*_j + \kappa_j$ so as to avoid any potential bias due to model simplification. The misfit of the spectral model to the data is minimized in the log–log space with the L2 norm. Using the resulting minimum misfit model, the residuals are then assumed to be an estimate of the normalized frequency-dependent elastic

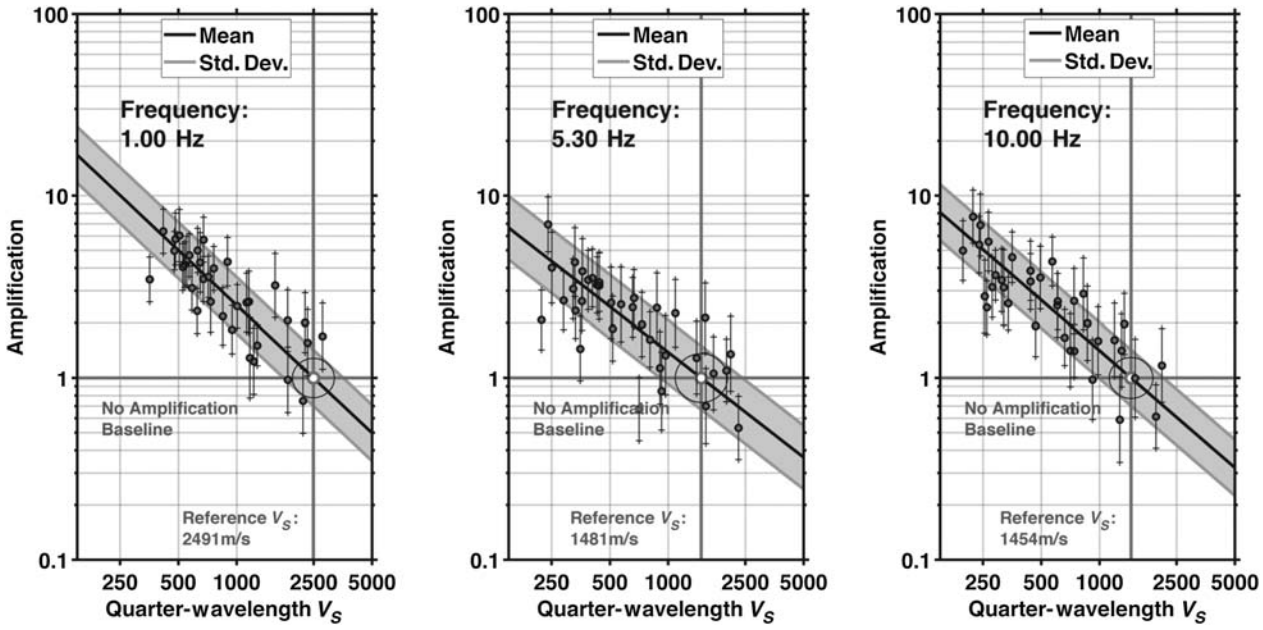

Figure 4. Correlation between quarter-wavelength (QWL) average velocities and amplification factors from spectral modeling of observed earthquake ground motion. A linear least-squares regression is applied in log–log space to estimate parameter dependency.

component of the site function, $a_j(f)$. Subsequently, by correcting for the geometric decay function (S_{ij} with fixed decay rate) the frequency-independent component of the modeled spectra—the signal moments—can be split into a single seismic moment M_0 and average site amplification terms A_j, relative to a common reference. Clearly however, a strong trade-off exists between the moment and average amplification. In order to decouple the site effect from the magnitude determination, M_w values determined by the U. S. Geological Survey are fixed, where available. This constraint has an impact on the reference, because we require hard-rock conditions at low frequencies in order to replicate the moment tensor M_w solution.

While this approach allows the simultaneous determination of the anelastic site-amplification function, the resulting elastic amplification may be subject to trade-off with $\kappa_{0,j}$. An alternative approach, simply fitting the high-frequency part of the spectrum above the source corner frequency, was proposed by Anderson and Hough (1984). For a given earthquake (i) and recording site (j), we can model the acceleration spectrum Ω_{ij} above the source corner frequency as

$$\ln[\Omega_{ij}(f)] = \ln[C_{ij}] - \pi f \kappa = \ln[C_{ij}] - \pi f[\kappa_{0,j} + \kappa_{ij}(R)], \tag{8}$$

in which f is the frequency, R is the distance, C_{ij} is a path-specific constant, and κ is the measured spectral decay (with respect to ω^2 high-frequency spectral displacement fall-off). Because we must fit only the spectra above the source corner frequency, we limited the data to recordings from magnitudes greater than 3.5 and fit the spectra between 10 and 30 Hz: the subset of data included a total of 15,801 geometric mean horizontal spectra from 1119 events. In order to minimize the trade-off between the source and site, the final anelastic function $[T_j(f, A_j, \kappa_j)]$ is produced from the product of A_j, $a_j(f)$ from the broadband inversion, and κ_j from the high-frequency fit (equation 6).

The Reference *S*-Wave Velocity Profile for Japan

A reference *S*-wave velocity profile for Japan can be obtained from the comparison of QWL average velocities at each specific seismic station locations with the corresponding empirical (elastic) amplification functions obtained from spectral modeling, following the procedure described in Poggi *et al.* (2011) for the Swiss network. As such, each average velocity estimate (versus depth) can be uniquely associated to a specific average amplification factor at a defined frequency (e.g., Fig. 4 at 1, 5.3, and 10 Hz). For the calibration, the 36 selected seismic station locations from the Japanese KiK-net network were used. From the ensemble of all measurement locations, amplification versus average velocity relationships (log–log linear correlations) were then established for a set of discrete frequencies between 1 and 10 Hz. Frequencies above and below this range were disregarded from the comparison, because of the progressive loss of resolution of the discrete velocity profile at large and very shallow depths.

In some cases the profiles did not reach a sufficient depth to cover the whole frequency range of the QWL computation. To solve this problem we make use of a cubic extrapolation procedure, as described in Edwards, Poggi, and Fäh (2011) and Poggi *et al.* (2011), to artificially extend the velocity information to a sufficient depth. It can be assumed that the procedure works sufficiently well in the case of rock sites, where a gradual gradient-like increase in velocity with depth is generally present. However, it might be

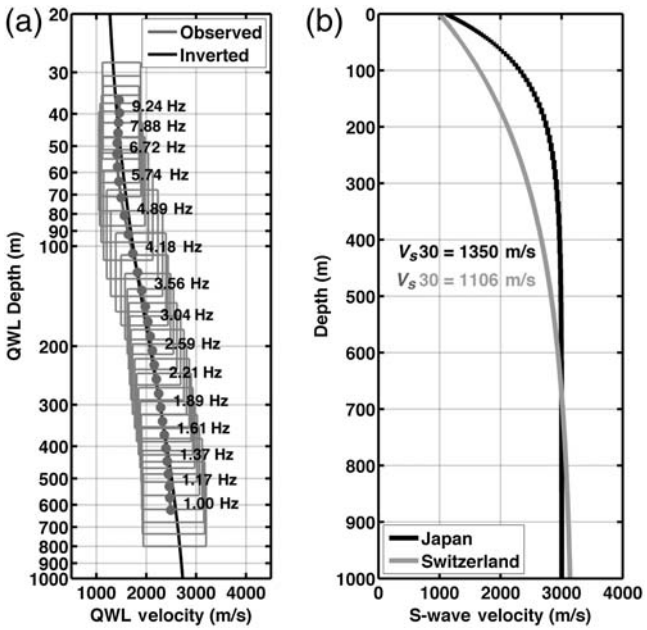

Figure 5. (a) QWL representation of the reference velocity profile obtained from the correlations between QWL average velocities and empirical amplification factors. (b) The inverted reference *S*-wave velocity profile in the more common velocity-depth representation, compared with the current Swiss reference rock profile.

problematic for some soft sediment sites to use such extrapolations, due to sharp contrasts of *S*-wave velocity that might be expected. We allowed for an extended extrapolation depth with a maximum corresponding to 0.2 times the depth of the last layer interface in the measured profile.

In a second step, assuming that the reference profile is defined by a lack of any relative amplification, the expected QWL average velocities corresponding to relative unitary amplification were extracted and collected from these relations separately. By collecting the average velocity estimates at the different frequencies, a QWL representation of the reference velocity profile is therefore established (Fig. 5a). However, for site characterization, a representation of the shear-wave velocity profile versus depth is required. This can be obtained through a nonlinear inversion procedure, searching for a suitable velocity profile whose QWL representation better explains the retrieved reference model. To describe the velocity profile, a simple gradient-like function can be used, such as

$$V_S(z) = (V_{S\max} - V_{S\min})[1 - b_1^{-z/b_2}] + V_{S\min}, \qquad (9)$$

in which coefficients b_1 and b_2 are curvature parameters and $V_{S\min}$ and $V_{S\max}$ are, respectively, the velocity constraints at the surface and at the standard reference depth of 4000 m (assuming an asymptotic behavior of the profile). The curvature coefficients and $V_{S\min}$ are directly obtained through global optimization, as outlined in Poggi *et al.* (2011), while the $V_{S\max}$ is prescribed *a priori* on the base of some considerations about the possible velocity variability in the Japanese basement and on the low-frequency part of the QWL reference profile. The final inverted profile shows a steep increase in velocity in the first 300 m, from about 1100 m/s ($V_{S\min}$) to almost 3000 m/s ($V_{S\max}$). Below a depth of 1000 m the velocity can be considered constant (Fig. 5b, Table 1).

Table 1
Parameters Used in Equation (9) to Construct the Shape of the Japanese Reference Velocity Profile in Gradient Form

$V_{S\min}$ (m/s)	$V_{S\max}$ (m/s)	b_1	b_2
1100	3000	24.54	322.33

The V_{S30} of the reference is about 1350 m/s, which identifies the profile as a hard-rock reference in standard V_{S30}-based classification schemes (e.g., NEHRP, Building Seismic Safety Council, 2003). Ozel *et al.* (1999) conclude that the near-surface velocity structure of Japan is complex with remarkable lateral velocity variations and with a high-velocity gradient reaching high V_S velocities within the first kilometer. This observation is confirmed with our reference profile.

The Site-Attenuation Model

For the 36 selected soil and rock sites of the Japanese network, attenuation term A^κ (function of the site and reference kappa, κ) of equation (6) was compared to the QWL average velocities in a range of discrete frequencies between 1 and 10 Hz, which is consistent with the reliability range used for the calibration of the reference profile. The goal is now to establish a parametric representation that gives us the possibility to predict the attenuation term from a set of known average velocities at an arbitrary site. In order to model the dependency between the two parameters, an exponential relation is proposed, with the following functional form:

$$\ln(A^K) = -\pi f \kappa = -c_1(f)(V_S^{\mathrm{QWL}})^{-c_2(f)}. \qquad (10)$$

Equation (10) was defined assuming an asymptotic behavior of the attenuation decay function, which should converge to 0 and 1 at respectively very low and very high velocities (Fig. 6). Introducing this prior to the model is advantageous, as it provides an additional constraint to the data fit, especially at high frequencies, where the larger scatter on the attenuation term is expected.

Using this representation, the regression coefficients c_1 and c_2 were determined for the selected frequency range (Fig. 7, Table 2). Uncertainty on the attenuation term is assumed to be lognormally distributed, and we therefore represent its standard deviation as multiplicative factor. From Figure 7 it is possible to notice that the scatter of the data increases at higher frequency, leading to larger uncertainties at frequencies corresponding to shallower depths. This is nevertheless expected, because of the exponential behavior of attenuation, where small changes in kappa are more evident at high frequencies.

By comparing the regression function at different frequencies, it is then possible to identify a clear trend (Fig. 8),

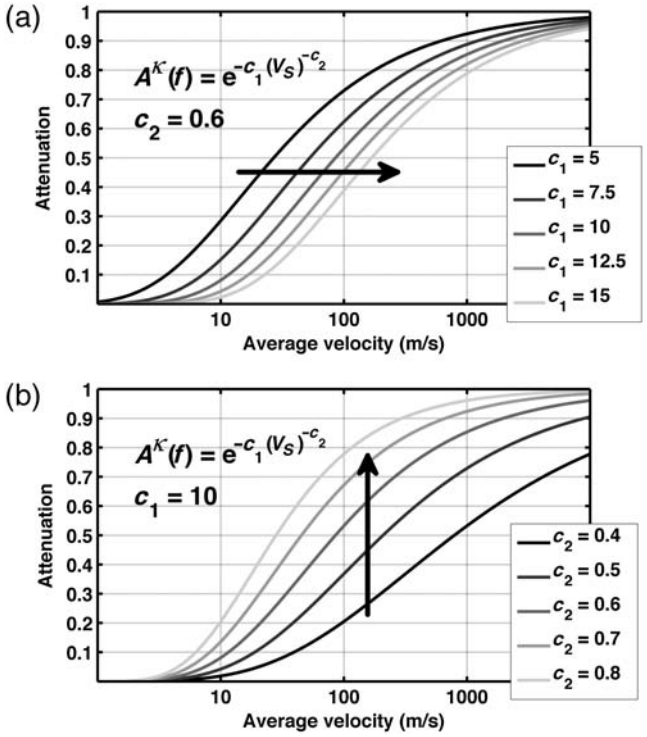

Figure 6. Example of influence on the attenuation–velocity regression model to the variation of the correlation coefficients c_1 and c_2. (a) c_1 is varied by keeping c_2 constant, leading to a progressive shift of the function toward high velocities. (b) Attenuation increases by progressively varying the c_2 coefficient.

which mostly affects coefficient c_1, while coefficient c_2 is rather stable at the average value of 0.48. Also the standard deviation follows a clear exponential trend over frequencies. This is of significance, because it gives the possibility to express the regression coefficients of equation (10) in a functional form, allowing the extrapolation of the attenuation term at any arbitrary frequencies within the calibration range (Fig. 9).

To model the variation of the regression coefficients over frequency different functional forms were tested. It was finally decided to use the following scheme:

$$\begin{cases} c_1 = d_1/(1 + (f/d_2)^{-d_3}) \\ c_2 = e_1 \log(f)^2 + e_2 \log(f) + e_3 \\ \text{Std.Dev.} = 1 + s_1 f^{s_2} \end{cases} . \qquad (11)$$

The parameters $d_{1–3}$, $e_{1–3}$, and $s_{1–2}$ of equation (11) were fitted through a nonlinear least-square regression, and the resulting values are given in Table 3. In a further simplification, the c_2 coefficient could be imposed to be constant at 0.48, given the relatively small variation of the parameter. This simplification, however, would make the extrapolation above and below the edge frequencies (1 and 10 Hz) questionable.

Obtaining the Kappa of the Reference

The established correlations between the attenuation factor A^κ and the QWL velocities are useful to predict the attenuation at any rock site for which the velocity profile or at least an estimate of the average velocity is available. The definition of the attenuation characteristics of the previously retrieved reference velocity profile is therefore straightforward. To do this, the QWL representation of the reference profile is first needed (Fig. 5a). For each analyzed discrete frequency and corresponding QWL velocity, a specific value of the frequency-dependent attenuation term A^κ is established (Fig. 10) using the functional form of equations (10) and (11). The uncertainty on the A^κ model can also be mapped over the different QWL velocities of the model. The ensemble of all A^κ values versus frequency defines the spectral exponential decay function of the reference (Fig. 11a). Subsequently, to obtain the single attenuation operator κ, a fitting procedure of the whole decay function is performed. The sensitivity of the decay function to kappa is given in Figure 11b for comparison. The uncertainty on the κ parameter can be obtained by fitting the standard deviation of the A^κ distribution of the reference. This, however, does not account for the uncertainty of the velocity profile—which is here not propagated—but only of the attenuation parameter. By applying this approach on the previously obtained Japanese reference velocity profile we obtain a value of κ of 0.022 ± 0.011 s. This value is somewhat higher than that estimated in Edwards, Fäh, and Giardini (2011), where a κ of 0.014 s was found for Swiss rock sites with V_{S30} of 1350 m/s. In Edwards and Fäh (2013), regressions between V_{S30} and κ for Swiss, Japanese, and other sites worldwide found κ of between 0.017 and 0.018 s (depending on the regression form adopted) for such a site. However, it should be noted that such linear regressions of V_{S30} against κ do not consider the physical justification of extrapolation, as in the current approach, instead relying on linear or log–linear extrapolation into poorly sampled model space.

Modeling the Anelastic Spectral Amplification of the Reference

From the retrieved Japanese reference profile, the elastic amplification function is now computed in a first step, using the 1D *SH*-wave transfer function formalism for vertical incidence (Fig. 12). For the computation, the Knopoff layer matrix formulation was used (Knopoff, 1964). The material density of the model was assumed to be constant with a value of 2500 kg/m^3, which appears to be a reasonable average estimate down to a depth of about 2000 m. Small variations in density would nevertheless affect the maximum amplification only by a negligible amount, as shown in Poggi *et al.* (2011).

Because the single Q_S values were not available at the different depths of the profile, it is not possible to compute the anelastic amplification by direct modeling of the visco-elastic *SH*-wave transfer function. Given the kappa value obtained for the reference, the frequency-dependent attenuation decay function A^κ was calculated and applied on top of the elastic amplification function (Fig. 12). It has to be mentioned that this simplified approach works generally well in the case of gradient-like rock profiles, where no visible

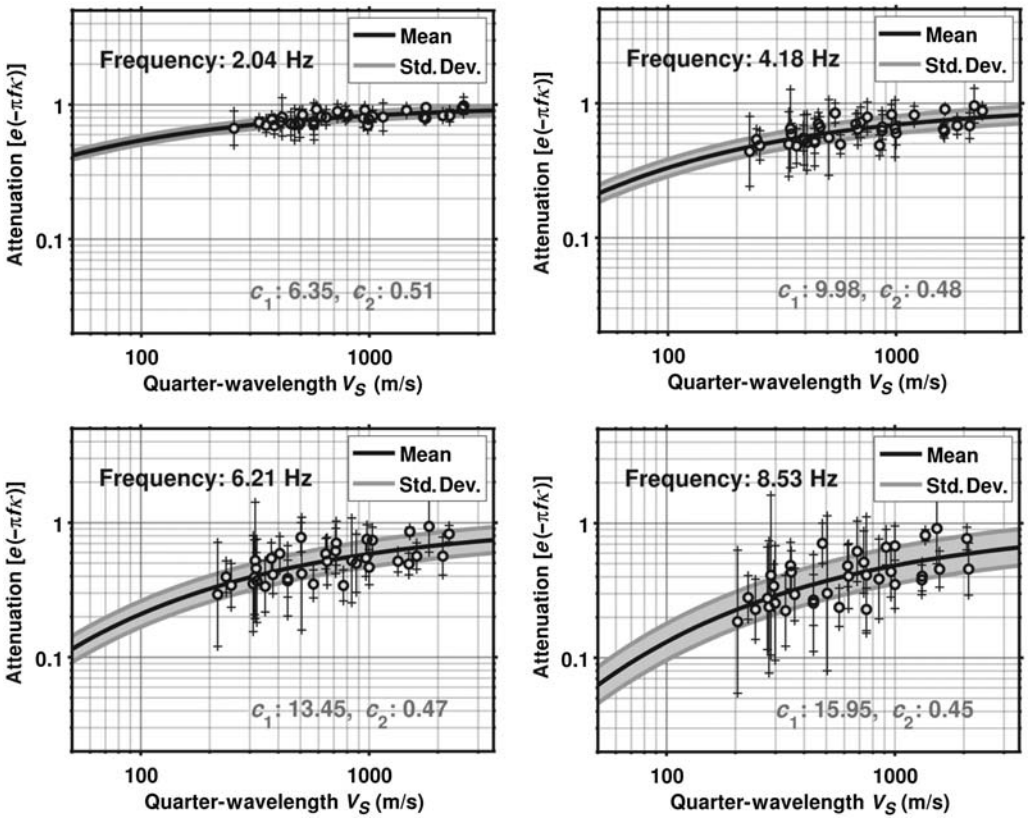

Figure 7. Correlation between QWL average velocity and attenuation (κ) for a set of discrete frequencies. The selection of 36 stations from KiK-net network is used. The scatter of the data becomes progressively important at increasing frequencies. Data uncertainty of the attenuation term is assumed to be log-normally distributed.

resonance effects are present, but it can be problematic when applied to soft sediment sites with strong resonances. The resulting anelastic amplification function now reaches a maximum amplification of about 1.12 at 3.5 Hz, which is a factor 1.5 less than in the elastic case.

Obtaining Kappa from V_{S30} Estimates

In general, obtaining κ with the proposed method is possible even if a single average velocity estimate is available at a given frequency (by using the QWL approach) or depth (by classic travel-time averaging). For the latter case, it is nevertheless always possible to retrieve the associated QWL frequency by considering the simple relation in equation (1). Therefore, by combining equation (1) within equations (10) and (11), it is then possible to associate a unique kappa value (and its uncertainty) to a single average velocity estimate. As a drawback, however, using a single velocity value might increase the final uncertainty of the final prediction, if compared to using the complete QWL representation of the velocity profile over a broad frequency range. In practice, single calibration points might be affected by a particularly large uncertainty and/or might not be fully representative of the whole velocity profile, leading to over-/underestimation of the final attenuation model.

We tested this approach on a range of V_{S30} values between 200 and 2000 m/s (Fig. 13), which corresponds to a range of QWL frequencies between about 1.67 and 16.67 Hz, according to equation (4). Clearly, V_{S30} values below 500 m/s are generally not representative of standard rock or stiff-soil conditions, for which the method is calibrated; investigating this extended range is nevertheless useful to obtain a first-order estimate of the minimum level of attenuation expected for these sites, without considering the attenuation related to the resonance of the seismic wavefield. Moreover, the results for high V_{S30} values are defined for frequencies outside the calibration range of the actual attenuation model and rely on the reliability of prediction model of equation (11) at high frequencies.

The results show a general trend of the prediction of κ with velocity, starting with a kappa of approximately 0.07 s at $V_{S30} = 200$ m/s and asymptotically converging to a value 0.02 s at $V_{S30} = 2000$ m/s. The standard deviation also progressively increases with the velocity. This can actually be justified by considering the variation in the corresponding QWL frequencies, which are higher at larger velocities. These estimates are nevertheless realistic, because they fall in the range of expectation for rock sites (Fig. 14). A particular advantage in this case, is that the relation between V_{S30} and κ is intrinsically parameterized based on the observed

Table 2
Regression Coefficients of the Attenuation–Velocity Relation (Equation 10) in the Range 1–10 Hz

Frequency (Hz)	c_1	c_2	σ^{κ}*
1.00	3.1078	0.4916	1.0384
1.08	3.3375	0.4919	1.0413
1.17	3.5450	0.4909	1.0445
1.27	3.6808	0.4865	1.0479
1.37	4.5045	0.5082	1.0515
1.49	4.8623	0.5095	1.0554
1.61	5.2487	0.5109	1.0596
1.74	5.5762	0.5098	1.0642
1.89	5.9322	0.5088	1.0693
2.04	6.3480	0.5085	1.0746
2.21	6.5807	0.5031	1.0809
2.40	6.8399	0.4980	1.0880
2.59	7.1397	0.4935	1.0957
2.81	7.5034	0.4899	1.1041
3.04	7.9856	0.4882	1.1129
3.29	8.3793	0.4843	1.1227
3.56	8.8704	0.4818	1.1333
3.86	9.3596	0.4790	1.1450
4.18	9.9794	0.4777	1.1577
4.52	10.7142	0.4772	1.1721
4.89	11.4503	0.4761	1.1881
5.30	12.1645	0.4742	1.2058
5.74	12.7918	0.4707	1.2257
6.21	13.4475	0.4671	1.2474
6.72	14.1068	0.4630	1.2718
7.28	14.7476	0.4583	1.2996
7.88	15.3865	0.4534	1.3307
8.53	15.9541	0.4476	1.3657
9.24	16.4349	0.4409	1.4057
10.00	16.8543	0.4336	1.4510

*Lognormal statistics are assumed to compute the standard deviation (σ^{κ}) of the attenuation regression model.

correspondence between QWL velocities and the attenuation, rather than on simple linear fitting as in previous studies (e.g., Silva *et al.*, 1998; Chandler *et al.*, 2006; Edwards and Fäh, 2013). Moreover, it has to be noticed that most of the existing V_{S30}–κ correlations are generally calibrated on datasets including both rock and soft sediment sites but without properly accounting for the presence of resonance phenomena. This is critical because, if a log–linear fit is used (e.g., Fig. 14), the effect of resonance at sites with rather low V_{S30} can influence the slope of the regression, which at high velocities values might then lead to particularly low values of κ for typical rock sites.

Discussion and Conclusions

In this paper we presented a method to obtain the characteristics of the reference rock conditions from a regional seismic network, including an estimate of its reference attenuation through the definition of the κ operator. The method is an extension of the procedure introduced by Poggi *et al.* (2011) for Switzerland and is here calibrated and applied to the Japanese KiK-net network. As a more general outcome of this study, the definition of a functional relation

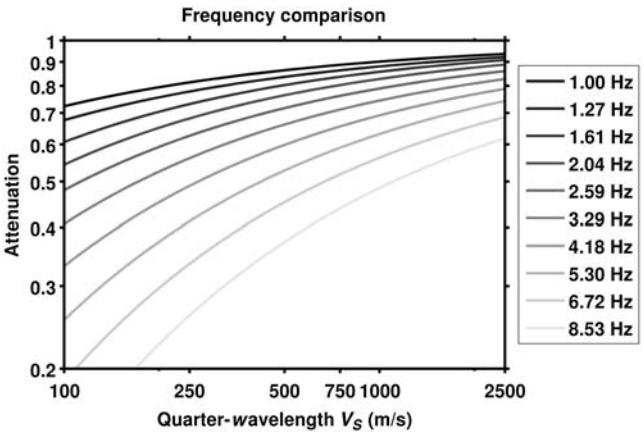

Figure 8. Comparison between κ correlations for the selected rock sites at discrete frequencies. It is evident a clear trend of the attenuation with increasing frequency at a given velocity, which is in agreement with rock-physics models.

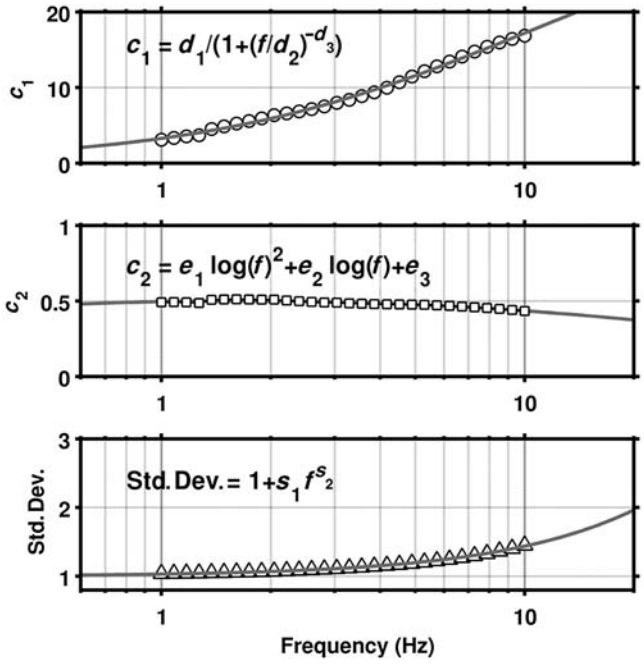

Figure 9. Variation of the regression coefficients (c_1 and c_2) and of the standard deviation over the frequency range 1–10 Hz. The fitted functional forms are presented as gray solid line.

to explain dependency between site attenuation and average QWL velocity gives the possibility to predict the attenuation characteristics of any rock profile for which a velocity profile or a corresponding average velocity representation are available. It has to be stressed, however, that even if such an approach demonstrated to be particularly suitable for those rock sites with a simple gradient form (like in the case of the Japanese reference profile), which produce a smooth predicted attenuation decay function, it might be problematic for those sites with strong velocity contrasts (e.g., a low-velocity layer close to the surface). In this case, the corresponding computed

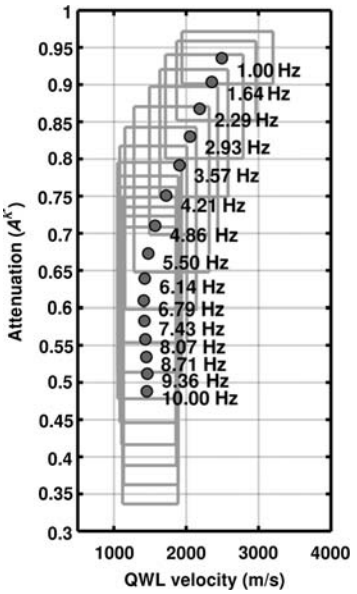

Figure 10. Attenuation values (A^κ) at the corresponding QWL velocities of the retrieved Japanese reference profile. Gray squares show the uncertainty of both the previously retrieved QWL reference (on the V_S^{QWL}) and of the attenuation regression model (on A^κ).

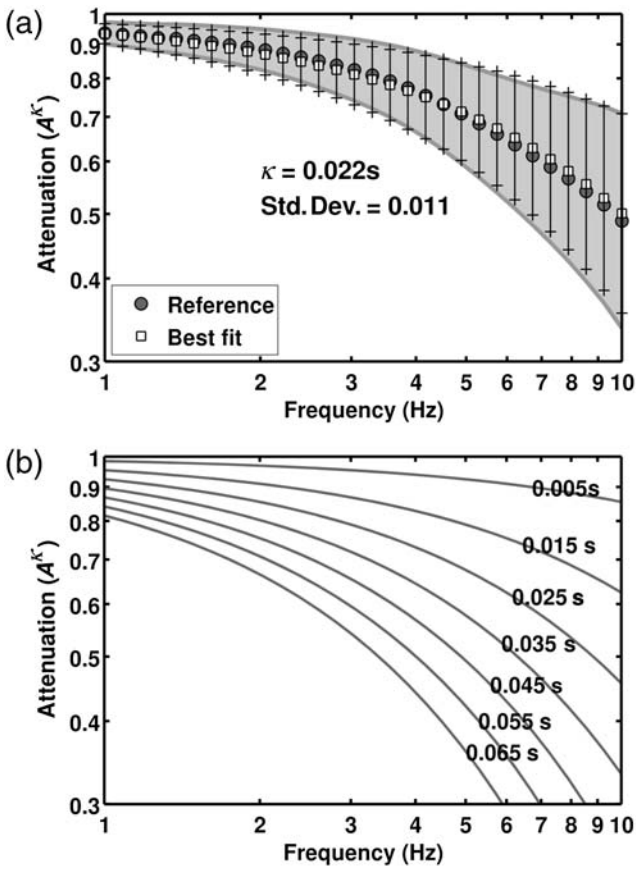

Figure 11. (a) Empirical decay function of the Japanese reference profile (gray circles) obtained from the correlation between QWL average velocities and attenuation factors (standard deviation in light gray). The corresponding best-fitting attenuation model ($\kappa = 0.022$ s) is shown by the square symbols, with the standard deviation represented by the error bars. (b) Attenuation decay function for a set of κ values between 0.005 and 0.065 s.

decay function might result in some step (or jump), leading to inconsistencies in the subsequent retrieval of κ from the attenuation function A^κ. Nevertheless, in such cases a simplification of attenuation in terms of the κ parameter may also be inappropriate. As well, it is not suggested to use such approach directly on soft-sediment sites, without also accounting for the resonance due to the strong velocity contrast between sediments and bedrock.

The reference rock profile obtained for Japan showed up to have rather high velocities at the surface (V_{S30} = 1350 m/s, corresponding to very-hard rock conditions) if compared to what was obtained for Switzerland. In first analysis, this dissimilarity can be addressed to evident differences in the tectonic context but can also be partially influenced by the selection of the seismic stations that were used to calibrate the reference in addition to the constraint of using M_w to decouple the retrieval of site-amplification parameters. Because our reference was chosen such that M_w from spectral inversion (e.g., Edwards *et al.*, 2010) were consistent with moment tensor inversion results, this requires that the reference is in fact very hard rock (with a general lack of amplification phenomena at low frequency). However, an additional reason for the high velocities may have been the presence in the selection of a number of stiff-soil sites with relatively low velocity ($V_{S30} < 1000$ m/s). This might have produced a shift of the frequency-dependent correlations toward slightly higher amplification factor at high frequencies, inducing consequently a shift of the velocity-unitary amplification intersection point to high velocities.

As additional outcome of the proposed method, a simplified approach to predict site attenuation from local V_{S30} was presented. By using this approach on a range of V_{S30} values up to 2000 m/s, realistic values of kappa were then obtained. The advantage of such procedure—if compared to directly correlating V_{S30} and κ—is that the intrinsic use of the QWL approach helps to separate and highlight the link between attenuation and site parameters at different resolution

Table 3
Coefficients Used to Fit the Functional Forms of Equation (11) to Observation

d_1	d_2	d_3	e_1	e_2	e_3	s_1	s_2
34.7463	10.2014	0.9741	−0.0202	0.0201	0.4957	0.0316	1.1420

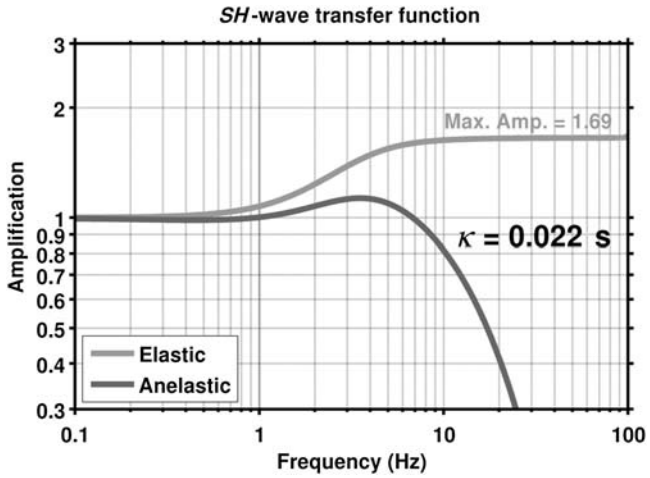

Figure 12. *SH*-wave amplification functions of the Japanese reference profile. The anelastic function is obtained from the elastic amplification by applying the attenuation decay from the inverted kappa model.

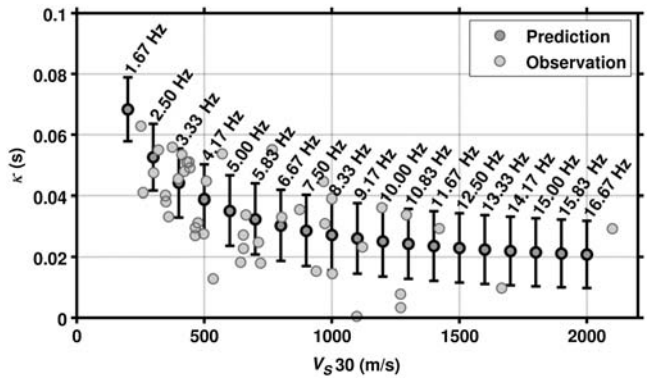

Figure 13. Predicted κ for a range of discrete V_{S30} velocities between 200 and 2000 m/s, which corresponds to an averaging frequency range between 1.67 and 16.67 Hz. The calibration dataset is visible in background as light-gray dots.

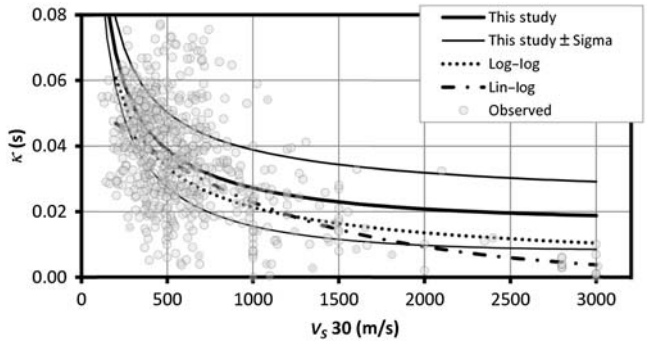

Figure 14. Comparison of the relation developed in this study with V_{S30}–κ data pairs from Japan, Switzerland, and worldwide (Silva *et al.*, 1998; Drouet *et al.*, 2010; Edwards, Fäh, and Giardini, 2011; Van Houtte *et al.*, 2011) and with a log–log and lin–log fit of data.

scales. This provides a more robust and physically based framework for the prediction; it therefore allows a justified extrapolation into poorly sampled model space (e.g., high V_{S30} sites). It has to be noticed, however, that the proposed V_{S30}–κ relation tends to converge to the value of 0.02 s at progressively increasing V_{S30} values ($V_{S30} > 1500$ m/s). This is a slightly higher value with respect to that which might be expected for very-hard rock sites, as seen in the comparison with real data. The standard deviation nevertheless increases as well, introducing a reasonable uncertainty to the expected value. At high velocities, we consider the κ values as an upper bound of possibilities. The asymptotic behavior of our V_{S30}–κ relation can be explained in different ways. As first, it has to be noticed that a general lack of data at rather high V_{S30} velocities exists, which might determine a constraint problem of the functional forms. On the other side, the extrapolation at high velocities (and in the case of V_{S30} also high frequencies) using the QWL approach has the advantage to be rather insensitive to lack of data at the edges of the regression, because of the assumed asymptotic behavior of the relation. As a further source of uncertainty it has to be mentioned that the quality of the extrapolation to high QWL velocities is strongly dependent on the resolution of the measured velocity profiles at the KiK-net stations, with special regard to the resolution at shallow depths. This information is in some cases incomplete, as a unique layer of average velocity is provided in the logs, therefore losing the necessary constraint for the regression at high frequencies. In some cases layers of weathered material are not resolved in the station profiles resulting in a possible bias to higher kappa values.

As a follow up of this study, we plan to explore the attenuation characteristics of soft-sediment sites, with the aim of establishing similar predictive equations to be used in sedimentary basins, including those particular sites with a strong velocity contrast to the underlying bedrock. This is nevertheless a more complex task, as the influence of additional phenomena (like the resonance) has to be properly accounted for in order to separate the different contributions to the anelastic attenuation. Additionally, we plan to use the relation between attenuation and average velocity to directly investigate the variability of *S*-wave quality factors (Q_S) in the rock velocity profiles.

Data and Resources

The Japanese earthquake data and velocity profiles are available through the NIED FTP service (http://www.kik.bosai.go.jp/; last accessed January 2011).

Acknowledgments

We thank the NIED for making waveform and velocity profile data available. This work was partly funded by swissnuclear through the PRP Project (Renault *et al.*, 2010) and the Swiss Federal Nuclear Safety Inspectorate (ENSI). We extend our thanks to reviewer Nicolas Kühn and Associate Editor Martin Chapman, whose comments helped significantly improve this paper.

References

Anderson, J. G., and S. E. Hough (1984). A model for the shape of the Fourier amplitude spectrum of acceleration at high-frequencies, *Bull. Seismol. Soc. Am.* **74,** 1969–1993.

Anderson, J. G., Y. J. Lee, Y. H. Zeng, and S. Day (1996). Control of strong motion by the upper 30 meters, *Bull. Seismol. Soc. Am.* **86,** 1749–1759.

Aoi, S., T. Kunugi, and H. Fujiwara (2004). Strong-motion seismograph network operated by NIED: K-Net and KiK-Net, *J. Japan Assoc. Earthq. Eng.* **4,** 65–74.

Atkinson, G. M., and D. M. Boore (2006). Earthquake ground-motion prediction equations for eastern North America, *Bul. Seismol. Soc. Am.* **96,** 2181–2205.

Atkinson, G. M., and R. Mereu (1992). The shape of ground motion attenuation curves in southeastern Canada, *Bull. Seismol. Soc. Am.* **82,** 2014–2031.

Boore, D. M., and W. B. Joyner (1997). Site amplifications for generic rock sites, *Bull. Seismol. Soc. Am.* **87,** 327–341.

Borcherdt, R. D. (1994). Estimates of site-dependent response spectra for design (methodology and justification), *Earthq. Spectra* **10,** 617–653.

Brune, J. N. (1970). Tectonic stress and the spectra of seismic shear waves from earthquakes, *J. Geophys. Res.* **75,** 4997–5010.

Brune, J. N. (1971). Correction: Tectonic stress and the spectra of seismic shear waves from earthquakes, *J. Geophys. Res.* **76,** 5002.

Building Seismic Safety Council (2003). The 2003 NEHRP recommended provisions for new buildings and other structures, Part 1: Provisions (FEMA 450), www.bssconline.org (last accessed October 2011).

Chandler, A. M., N. T. K. Lam, and H. H. Tsang (2006). Near-surface attenuation modelling based on rock shear-wave velocity profile, *Soil Dynam. Earthq. Eng.* **26,** 1004–1014.

Delavaud, E., F. Cotton, S. Akkar, F. Scherbaum, L. Danciu, C. Beauval, S. Drouet, J. Douglas, R. Basili, M. A. Sandikkaya, M. Segou, E. Faccioli, and N. Theodoulidis (2012). Toward a ground-motion logic tree for probabilistic seismic hazard assessment in Europe, *J. Seismol.* **16,** 451–473.

Dobry, R., R. D. Borcherdt, C. B. Crouse, I. M. Idriss, W. B. Joyner, G. R. Martin, M. S. Power, E. E. Rinne, and R. B. Seed (2000). New site coefficients and site classification system used in recent Building Seismic Code provisions, *Earthq. Spectra* **16,** 41–67.

Drouet, S., F. Cotton, and P. Gueguen (2010). nu(S30), kappa, regional attenuation and M-w from accelerograms: Application to magnitude 3–5 French earthquakes, *Geophys. J. Int.* **182,** 880–898.

Edwards, B., and D. Fäh (2013). Measurements of stress parameter and site attenuation from recordings of moderate to large earthquakes in Europe and the Middle East, *Geophys. J. Int.* doi: 10.1093/gji/ggt158.

Edwards, B., B. Allmann, D. Fäh, and J. Clinton (2010). Automatic computation of moment magnitudes for small earthquakes and the scaling of local to moment magnitude, *Geophys. J. Int.* **183,** 407–420.

Edwards, B., D. Fäh, and D. Giardini (2011). Attenuation of seismic shear wave energy in Switzerland, *Geophys. J. Int.* **185,** 967–984.

Edwards, B., C. Michel, V. Poggi, and D. Fäh (2013). Determination of site amplification from regional seismicity: Application to the Swiss National Seismic Networks, *Seismol. Res. Lett.* **84,** no. 4, 611–621, doi: 10.1785/0220120176.

Edwards, B., V. Poggi, and D. Fäh (2011). A predictive equation for the vertical-to-horizontal ratio of ground motion at rock sites based on shear-wave velocity profiles from Japan and Switzerland, *Bull. Seismol. Soc. Am.* **101,** 2998–3019.

Edwards, B., A. Rietbrock, J. J. Bommer, and B. Baptie (2008). The acquisition of source, path, and site effects from microearthquake recordings using Q tomography: Application to the United Kingdom, *Bull. Seismol. Soc. Am.* **98,** 1915–1935.

European Committee for Standardization (CEN) (2004). Eurocode 8: Design of structures for earthquake resistance—Part 1: General rules, seismic actions and rules for buildings. Bruxelles.

Joyner, W. B., R. E. Warrick, and T. E. Fumal (1981). The effect of quaternary alluvium on strong ground motion in the Coyote Lake, California, earthquake of 1979, *Bull. Seismol. Soc. Am.* **71,** 1333–1349.

Knopoff, L. (1964). A matrix method for elastic wave problems, *Bull. Seismol. Soc. Am.* **54,** 431–438.

Özel, O., T. Iwasaki, T. Moriya, S. Sakai, T. Maeda, C. Piao, Y. Yoshii, S. Tsukuda, A. Ito, M. Suzuki, A. Yamazaki, and H. Miyamachi (1999). Crustal structure of central Japan and its petrological implications, *Geophy. J. Int.* **138,** 257–274.

Poggi, V., B. Edwards, and D. Fäh (2011). Derivation of a reference shear-wave velocity model from empirical site amplification, *Bull. Seismol. Soc. Am.* **101,** 258–274.

Poggi, V., B. Edwards, and D. Fäh (2012), Characterizing the vertical-to-horizontal ratio of ground motion at soft-sediment sites, *Bull. Seismol. Soc. Am.* **102,** 2741–2756.

Renault, P., S. Heuberger, and N. A. Abrahamson (2010), PEGASOS Refinement Project: An improved PSHA for Swiss nuclear power plants, in *Proc. of 14th ECEE—European Conference on Earthquake Engineering*, Ohrid, Republic of Macedonia, 30 August–3 September, Paper ID 991.

Silva, W., R. Darragh, N. Gregor, G. Martin, N. Abrahamson, and C. Kircher (1998). Reassessment of site coefficients and near-fault factors for building code provisions, Technical report program element II: 98-HQGR-1010, *Pacific Engineering and Analysis*, El Cerrito, USA.

Van Houtte, C., S. Drouet, and F. Cotton (2011). Analysis of the origins of κ (Kappa) to compute hard rock to rock adjustment factors for GMPEs, *Bull. Seismol. Soc. Am.* **101,** 2926–2941.

Swiss Seismological Service
Sonneggstrasse, 5
ETH Zürich
Zürich, Switzerland
poggi@sed.ethz.ch

Manuscript received 21 December 2012